ResearchGate

See discussions, stats, and author profiles for this publication at: https://www.researchgate.net/publication/231654191

High-k Tm2O3 Sensing Membrane-Based Electrolyte–Insulator–Semiconductor for pH Detection

ARTICLE *in* THE JOURNAL OF PHYSICAL CHEMISTRY C · DECEMBER 2009

Impact Factor: 4.77 · DOI: 10.1021/jp908129k

CITATIONS
12

READS
20

3 AUTHORS, INCLUDING:

Tung-Ming Pan
Chang Gung University
212 PUBLICATIONS **1,370** CITATIONS
SEE PROFILE

Min-Hsien Wu
Chang Gung University
74 PUBLICATIONS **1,016** CITATIONS
SEE PROFILE

Available from: Tung-Ming Pan
Retrieved on: 17 January 2016

High-k Tm_2O_3 Sensing Membrane-Based Electrolyte−Insulator−Semiconductor for pH Detection

Tung-Ming Pan,*,†,‡ Cheng-Da Lee,†,‡ and Min-Hsien Wu‡,§

Department of Electronics Engineering, Chang Gung University, Taoyuan 333, Taiwan, Republic of China, Bio-Sensor Group, Bio-Medical Engineering Research Center, Chang Gung University, Taoyuan 333, Taiwan, Republic of China, and Graduate Institute of Biochemical and Biomedical Engineering, Chang Gung University, Taoyuan 333, Taiwan, Republic of China

Received: August 23, 2009; Revised Manuscript Received: November 12, 2009

For high-sensitive pH sensing, an electrolyte−insulator−semiconductor (EIS) device with a Tm_2O_3 sensing membrane fabricated by reactive sputtering and the succeeding postdeposition annealing treatment was proposed. In this study, the influence of thermal annealing (700, 800, and 900 °C) on the structural characteristics of the Tm_2O_3 sensing membrane was investigated by X-ray diffraction, atomic force microscopy, and X-ray photoelectron spectroscopy. The observed structural properties were then correlated with the resulting pH-sensing performance. Results revealed that the EIS device with a Tm_2O_3 sensing film annealed at 800 °C exhibited a higher sensitivity of 58.02 mV/pH (within the pH range of pH 2−12), a lower hysteresis voltage of 2 mV (measurement cycle, pH = 7→4→7→10→7), and a lower drift rate of 1.04 mV/h (at the condition of pH 7) compared with those at other annealing temperatures. These results are attributed to the formation of a well-crystallized Tm_2O_3 structure, a thinner low-k interfacial layer at the oxide/Si interface, and the higher surface roughness at such thermal annealing conditions. As a whole, this study provided some fundamental data regarding the application of Tm_2O_3 sensing membrane-based EIS devices for pH detection.

Introduction

Ion-sensitive field-effect transistor (ISFET) devices have been studied extensively for the chemical sensing of ion concentrations in solution (e.g., H^+, Cl^-, Na^+, K^+, NH_4^+, Ca^{2+}, etc.) because of their distinctive advantages of compact size, low cost, rapid response, ease of fabrication, and, particularly, the high compatibility for integration with complementary metal oxide semiconductors (CMOSs).[1] Metal oxide semiconductor field-effect transistor (MOSFET) devices consist mainly of the metal, the oxide, the source/drain, and the semiconductor substrate; the difference between an ISFET and an MOSFET device is that no metal gate electrode is employed in the former. The original SiO_2 material used as a pH-sensitive membrane for ISFETs was introduced by Bergveld[2] in 1970. Si_3N_4 film is the most popular material for a sensing membrane because of its easy process and high compatibility for CMOS integration.[3] The disadvantage of Si_3N_4 film is the degradation of pH-sensing characteristics due to the surface oxidation. High-k dielectric materials, including Al_2O_3, Ta_2O_5, TiO_2, HfO_2, ZrO_2, and Gd_2O_3,[4−9] have been proposed as a sensing membrane for pH-ISFET application because of their higher pH response. To improve the quality of the interface between the high-k material and the silicon substrate, growing a thin SiO_2 film on the Si substrate imparts the pH-sensing membrane with a lower density of the interfacial state, smaller stress, and good adhesion.[10]

Recently, rare-earth oxide thin films have been investigated for semiconductor applications due to high dielectric constants, high resistivities, and large energy band gap characteristics.[11,12] A thulium oxide (Tm_2O_3) film can be considered as a sensing film in the pH-ISFET devices because of its dielectric constant of ∼13, energy band gap of >5 eV, and predicted chemical and thermal stability with Si.[13,14] Furthermore, Paivasaari et al.[15] showed the electrical characteristics and physical properties of Tm_2O_3 thin film grown onto a silicon(100) substrate using atomic layer deposition. In this article, we describe the physical and sensing characteristics of thin Tm_2O_3 sensing films deposited on Si substrates by means of reactive sputtering. We have used X-ray diffraction (XRD) to monitor the growth directions and crystallinity of the films and X-ray photoelectron spectroscopy (XPS) to determine the chemical structure of the Tm_2O_3 films after annealing at various temperatures. The surface roughness of Tm_2O_3 sensing films after different annealing temperatures was characterized with atomic force microscopy (AFM). Furthermore, we discuss the effects of annealing on the sensing characteristics of Tm_2O_3 electrolyte−insulator−semiconductor (EIS) devices.

Experimental Section

The EIS devices incorporating Tm_2O_3 sensing membranes were fabricated 4 inch p-type Si(100) wafers. Before the deposition of Tm_2O_3, the wafers were cleaned with a standard RCA and then they were treated with 1% HF to remove the native oxide. An ∼25 nm Tm_2O_3 film was deposited on a Si substrate by reactive sputtering from a thulium target with a base pressure of about 10^{-6} Torr. Samples were annealed at different temperatures by rapid thermal annealing (RTA) in O_2 ambient for 30 s. The backside contact (a 400 nm thick Al film) of the Si wafer was deposited using a thermal coater. The sensing membrane size was defined through photolithographic processing under a photosensitive epoxy (SU8-2005, Micro-Chem) that behaved as an antiacid polymer. EIS devices were then fabricated on the Cu lines of a printed circuit board using

* To whom correspondence should be addressed. Tel: 886-3-211-8800, ext. 3349. Fax: 886-3-211-8507. E-mail: tmpan@mail.cgu.edu.tw.
† Department of Electronics Engineering.
‡ Bio-Medical Engineering Research Center.
§ Graduate Institute of Biochemical and Biomedical Engineering.

10.1021/jp908129k © 2009 American Chemical Society
Published on Web 12/10/2009

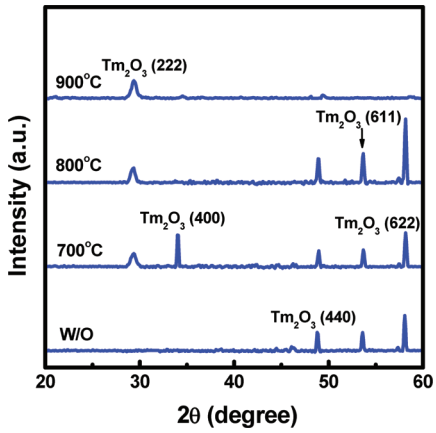

Figure 1. XRD of Tm_2O_3 dielectric films annealed at different temperatures.

a Ag gel to form conductive lines. A handmade epoxy package was used to encapsulate the EIS structure and the Cu line.

The film structure and composition of Tm_2O_3 dielectric films with postdeposition annealing (PDA) at various temperatures were analyzed by XRD and XPS. The surface morphologies of the Tm_2O_3 sensing dielectrics were analyzed by AFM. The pH sensitivities of the Tm_2O_3 sensing membranes were determined by measuring capacitance—voltage ($C-V$) curves of the EIS devices. The $C-V$ curves were measured using buffer solutions of various values of pH (Merck Inc.), a Ag/AgCl reference electrode, and a Hewlett-Packard 4284A LCR meter operated at an ac signal frequency of 100 Hz to maintain the electrochemical system at equilibrium. All setups were performed in a dark box to avoid interference from light and noise.

Results and Discussion

To study the crystalline structures and orientations of Tm_2O_3 films annealed at different temperatures, XRD measurements were conducted (Figure 1). The XRD patterns indicate that the films comprise the cubic phase of the Tm_2O_3 film. The as-deposited (W/O) film exhibits three (400), (611), and (622) peaks. The temperature-induced evolution of the crystalline structure of the Tm_2O_3 film can be followed by XRD analysis. The sample annealed at 700 °C exhibited three small (222), (440), and (611) peaks, and two large (400) and (622) peaks, whereas the sample prepared at 800 °C had a strong (622) peak and three weak (222), (440), and (611) peaks. This suggests a preferential orientation of the crystallites with the (622) planes of cubic Tm_2O_3 parallel to the substrate for the 800 °C annealed case. The intensities of these peaks, except for the (400) peak, increase upon the RTA temperature. This is due to crystallization and/or grain growth during high-temperature annealing. The film annealed at 900 °C showed only a preference for the (222) crystallographic orientation, as shown in Figure 1. This result suggests the formation of a low-k interfacial layer at the Tm_2O_3/Si interface due to the diffusion of thulium and oxygen from the film to the Si substrate.

The surface roughness of the Tm_2O_3 sensing films after RTA at different temperatures is shown in Figure 2. The as-deposited Tm_2O_3 film exhibited a smaller surface roughness than the annealed film. Moreover, the surface roughness of the Tm_2O_3 films clearly increased upon increasing the RTA temperature but suddenly decreased at 900 °C. The availability of defect sites due to higher density can enhance self-diffusion of thulium and oxygen, causing larger grain-boundary velocity during annealing and, therefore, large grains. It is worth mentioning that the sample annealed 900 °C shows a lower surface roughness compared with 800 °C. This is attributed to the fact that the thulium atoms removed from the oxide film mostly migrated to the oxide/Si interface during high-temperature annealing, thus resulting in a small roughness surface.

We used XPS to analyze the structural and compositional changes in the Tm_2O_3 films as a function of the annealing temperature. Figure 3a shows the Tm $4d_{5/2}$ XPS spectra of the Tm_2O_3 films annealed at different RTA temperatures. The Tm $4d_{5/2}$ peak of the Tm_2O_3 reference is located at 175.6 eV.[16] The as-deposited film shifted the peak position to a higher binding energy by approximately 0.6 eV relative to the Tm_2O_3 reference

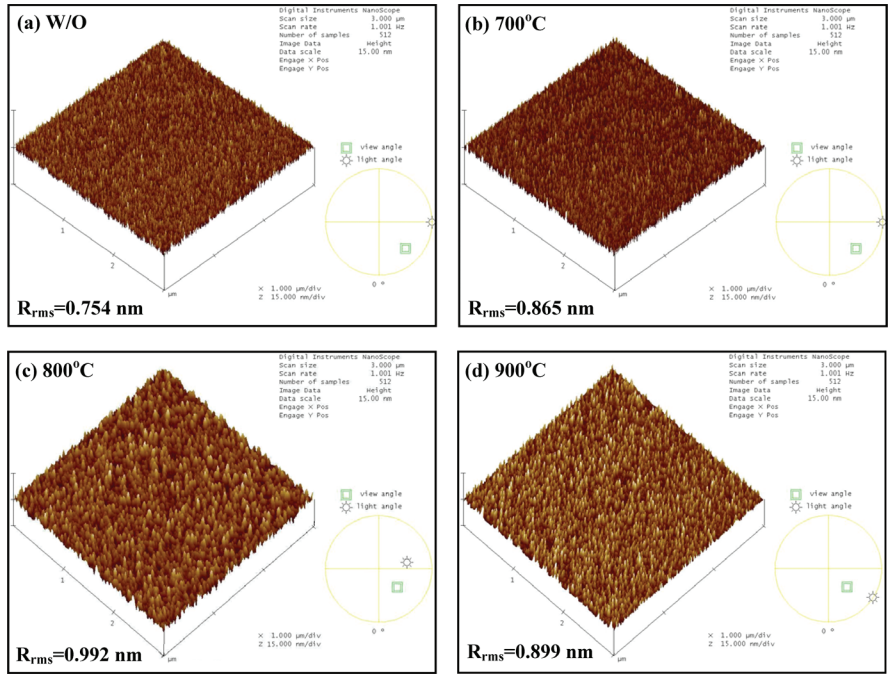

Figure 2. AFM surface image of Tm_2O_3 sensing films for (a) as-deposited and annealed at (b) 700 °C, (c) 800 °C, and (d) 900 °C.

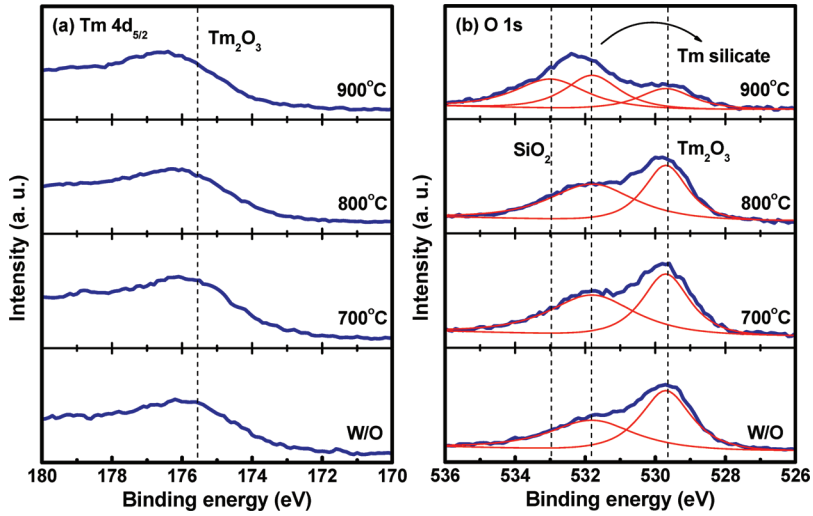

Figure 3. (a) Tm 4d and (b) O 1s XPS spectra of Tm_2O_3 films annealed at different temperatures.

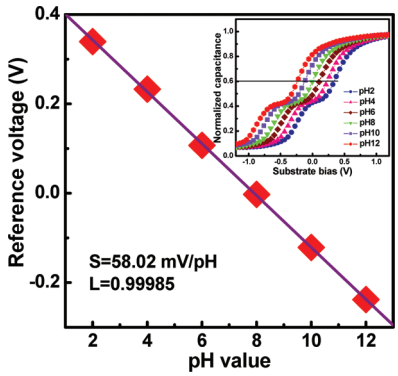

Figure 4. Reference voltage of Tm_2O_3 EIS device prepared through RTA at 800 °C plotted as a function of pH at room temperature. Inset: *C*−curves displaying the response of the Tm_2O_3 sensing films annealed at 800 °C when submerged into solutions at values of pH ranging from 2 to 12.

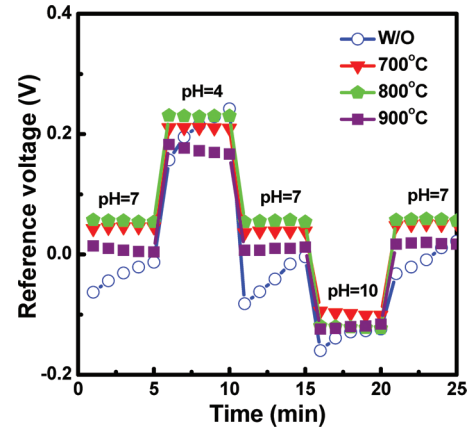

Figure 5. Hysteresis voltage of Tm_2O_3 EIS devices annealed at different temperatures during the pH = 7→4→7→10→7.

TABLE 1: Surface Roughness of AFM and pH Response Parameters for All Samples, Including Sensitivity, Hysteresis Voltage, and Drift Rate

PDA temperature (°C)	surface roughness (nm)	sensitivity (mV/pH)	hysteresis voltage (mV)	drift rate (mV/h)
W/O	0.754	48.63	29	17.4
700	0.865	53.40	5	2.80
800	0.992	58.02	2	1.04
900	0.899	55.90	10	3.60

position, suggesting Tm silicate (TmO_xSi_y) formation at the interface during film deposition. At annealing temperatures up to 800 °C, it was found that the Tm 4d peak position was almost no change in binding energy and that there was a sudden increase in the shift after annealing at 900 °C. This is due to the presence of a thicker low-*k* interfacial layer. Figure 3b displays the O 1s energy level region in the XPS spectra of the samples after RTA at different temperatures. A multipeak Lorentzian−Gaussian deconvolution procedure was used to extract the exact line position and intensities. When peak fitting was necessary to locate peak position or integrate area, Lorentzian−Gaussian functions were generated by minimizing the misfit error. The O 1s signal comprised three peaks at 529.7, 531.8, and 533 eV, which we assign to Tm_2O_3,[16] Tm silicate, and SiO_2,[17] respectively. The O 1s peak intensity corresponding to Tm_2O_3 is rather constant up to 800 °C but suddenly decreases

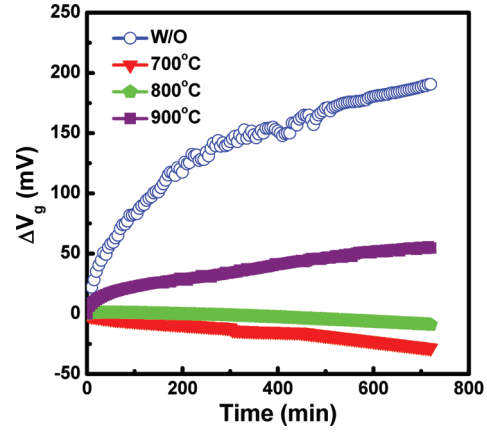

Figure 6. Drift characteristics of Tm_2O_3 EIS capacitors annealed at different temperatures as a function of time in the pH = 7 solution.

at 900 °C, while the O 1s peak intensity corresponding to SiO_2 suddenly increases at 900 °C. For annealing performed at 900 °C, the Si, O, and Tm atoms that diffused from the Tm_2O_3 film reacted with the Si substrate to form silica and Tm silicate, as suggested by the sudden increase in the O 1s peak intensity corresponding to SiO_2 and/or Tm silicate and the decrease in the O 1s peak intensity corresponding to Tm_2O_3. The SiO_2 layer grew monotonically at the film/Si interface owing to the oxygen diffusion toward the interface from the crystal defect and nonstoichiometric structure with the high-temperature RTA.[18]

A group of $C-V$ curves as a function of various pH solutions were measured to estimate the pH sensitivity of the Tm_2O_3 sensing membrane. Changing the pH of the solution led to a shift in the flat-band voltage of the $C-V$ curves. As a result of the shift, a group of $C-V$ curves can be obtained as a function of pH value. This behavior can be explained by using the site-binding model[19] to describe the ionic absorption processes at the electrolyte/oxide interface. The reference voltages are obtained from the $C-V$ curves for achieving the normalized capacitance of 0.6. The results indicate the shift of reference voltage for Tm_2O_3 sensing films during a cycle of experiments from pH 2 to pH 12, as shown in Figure 4. These $C-V$ curves were shifted as a result of the surface potential modification by the formation of a hydrogen ion dipole on the sensing film. It is found that Tm_2O_3 EIS devices annealed at 800 °C exhibited a high pH sensitivity of 58.02 mV/pH and good linearity. The inset of Figure 4 illustrates one group of $C-V$ curves of the EIS device incorporating a high-k Tm_2O_3 sensing film after PDA at 800 °C in different pH buffer solutions. It is found that a Tm_2O_3 EIS device annealed at 800 °C exhibited a better pH sensitivity than those of the devices performed at the other RTA temperatures, as shown in Table 1. This result could be attributed to the higher surface roughness of the Tm_2O_3 sensing membrane annealed at 800 °C, as observed in the previous AFM analysis. With the higher surface roughness, the N_s will increase accordingly, which, therefore, contributes to higher detection sensitivity, as previously reported in the site-binding model.[7]

Hysteresis can be due to the defects of a dielectric film, causing the formation of porous structures. The interior sites of these porous defects could react with the ions existing in the tested solution and thus cause a hysteresis response. Another possible cause is the interaction of ions in the solution with the responding sites along the boundaries of grains on an insulator film.[20] We subjected the EIS capacitors using a Tm_2O_3 sensing film to the pH loop of 7→4→7→10→7 over a period of 1500 s. A smaller hysteresis voltage of the Tm_2O_3 sensing films after RTA at 800 °C is 2 mV in the pH loops of 7→4→7→10→7, as shown in Figure 5. This may be due to the well-crystallized Tm_2O_3 structure.

The drift rate of pH-ISFET is described using a hopping and/or trap-limited transport mechanism, also known as dispersive transport,[21,22] to evaluate the hydration rate of the insulator. The phenomena of dispersive transport can be found in a broad class of disordered materials. In an amorphous material, for example, dispersive transport may result from hopping motion through localized states (hopping transport), trap-limited transport in the presence of traps possessing an exponential energy distribution (multiple-trap transport), or a combination of the aforementioned transport mechanisms (trap-controlled hopping transport).[22] Dispersive transport causes a decay in the density of sites/traps occupied by the species going through transport.[23] The hypothesis that hydration of the gate dielectric is controlled by a dispersive transport mechanism is sustained by the presence of buried surface sites and/or the presence of traps (specifically electrically active silicon dangling bonds). The variations in the chemical composition of the insulator surface give rise to the change in number of surface sites with time, thus causing a monotonic temporal increase in the threshold voltage. Figure 6 displays the drift rate of a high-k Tm_2O_3 sensing membrane after RTA at temperatures as a function of time, measured in the pH 7 solutions for 12 h. The EIS capacitor annealed 800 °C showed the best long-term stability (1.04 mV/h); in contrast, the EIS device without PDA treatment featured a serious drift of 17.4 mV/h. The improvement in the drift characteristics was accomplished on the formation of a silicate layer at the oxide/Si interface and well-crystallized Tm_2O_3 structure. However, a higher drift rate was considered to be caused by the presence of a high density of crystal defects.

Conclusion

In this article, we studied the structural and sensing characteristics of Tm_2O_3 sensing films grown on the Si(100) substrate by means of reactive sputtering. The presence of a Tm_2O_3 structure in the EIS device was confirmed by means of XRD, AFM, and XPS analysis. We find that the EIS device incorporating a high-k Tm_2O_3 film with subsequent RTA at 800 °C exhibited a high sensitivity of 58.02 mV/pH in the solutions from pH 2 to pH 12, a low hysteresis voltage of 2 mV in the pH = 7→4→7→10→7, and a small drift rate of 1.04 mV/h in the pH 7 buffer solution. This can be explained by the presence of a well-crystallized Tm_2O_3 structure, a large surface roughness, and a thin Tm silicate layer. EIS devices incorporating a high-k Tm_2O_3 sensing membrane show promise for use in pH-ISFET applications.

Acknowledgment. This work was supported by the National Science Council, Taiwan, Republic of China, under Contract No. NSC-97-2111-E-182-050-MY3.

References and Notes

(1) Bergveld, P. *Sens. Actuators, B* **2003**, *88* (1), 1–20.
(2) Bergveld, P. *IEEE Trans. Biomed. Eng.* **1970**, *17* (1), 70–71.
(3) Chen, K. M.; Li, G. H.; Chen, L. X.; Zhu, Y. *Sens. Actuators, B* **1993**, *13* (1−3), 209–211.
(4) Matsuo, T.; Esashi, M.; Abe, H. *IEEE Trans. Electron Devices* **1979**, *26* (11), 1856–1857.
(5) Fog, A.; Buck, R. P. *Sens. Actuators* **1984**, *5* (2), 137–146.
(6) Poghossian, A.; Schoning, M. J. *Electroanalysis* **2004**, *16* (22), 1863–1872.
(7) Lai, C. S.; Yang, C. M.; Lu, T. F. *Electrochem. Solid-State Lett.* **2006**, *9* (3), G90–G92.
(8) Yoshida, S.; Hara, N.; Sugimoto, K. *J. Electrochem. Soc.* **2004**, *151* (3), H53–H58.
(9) Chang, L. B.; Ko, H. H.; Jeng, M. J.; Lee, Y. L.; Lai, C. S. *J. Electrochem. Soc.* **2007**, *154* (5), J150–J154.
(10) Wilk, G. D.; Wallace, R. M.; Anthony, J. M. *J. Appl. Phys.* **2001**, *89* (10), 5243–5275.
(11) Scarel, G.; Debernardi, A.; Tsoutsou, D.; Spiga, S.; Capelli, S. C.; Lamagna, L.; Volkos, S. N.; Alia, M.; Fanciulli, M. *Appl. Phys. Lett.* **2007**, *91* (10), 102901.
(12) Kwo, J.; Hong, M.; Kortan, A. R.; Queeney, K. T.; Chabal, Y. J.; Mannaerts, J. P.; Boone, T.; Krajewski, J. J.; Sergent, A. M.; Rosamilia, J. M. *Appl. Phys. Lett.* **2000**, *77* (1), 130–132.
(13) Shannon, R. D. *J. Appl. Phys.* **1993**, *73* (1), 348–366.
(14) Iwai, H.; Ohmi, S.; Akama, S.; Ohshima, C.; Kikuchi, A.; Kashiwagi, I.; Taguchi, J.; Yamamoto, H.; Tonotani, J.; Kim, Y.; Ueda, I.; Kuriyama, A.; Yoshihara, Y. *Technical Digest IEEE International Electron Devices Meeting*, 2002; pp 625−628.
(15) Paivasaari, J.; Putkonen, M.; Niinist, L. *Thin Solid Films* **2005**, *472* (1−2), 275–281.
(16) Dzhurinskii, B. F.; Gati, D.; Sergushin, N. P.; Nefedov, V. I.; Salyn, Y. V. *Russ. J. Inorg. Chem.* **1975**, *20* (8), 2307–2314.
(17) Moulder, J. F.; Stickle, W. F.; Sobol, P. E.; Bomben, K. D. *Handbook of X-Ray Photoelectron Spectroscopy: A Reference Book of Standard Spectra for Identification and Interpretation of XPS Data*; Physical Electronics Inc.: Chanhassen, MN, 1995.
(18) Fanciulli, M.; Scarel, G. *Rare Earth Oxide Thin Film: Growth, Characterization, and Applications*; Springer: Berlin, 2007.
(19) Shinwari, M. W.; Deen, M. J.; Landheer, D. *Microelectron. Reliab.* **2007**, *47* (12), 2025–2057.
(20) Bousse, L.; van der Vlekkert, H. H.; de Rooij, N. F. *Sens. Actuators, B* **1990**, *2* (2), 103–110.
(21) Scher, H.; Montroll, E. W. *Phys. Rev. B* **1975**, *12* (6), 2455–2477.
(22) Pfister, G.; Scher, H. *Phys. Rev. B* **1977**, *15* (4), 2062–2083.
(23) Kakalios, J.; Street, R. A. W.; Jackson, B. *Phys. Rev. Lett.* **1987**, *59* (9), 1037–1040.

JP908129K